Journal: Monthly Notices of the Royal Astronomical Society
Article doi: 10.1093/mnras/stw099
Article title: Nuclear discs as clocks for the assembly history of early-type galaxies: the case of NGC 4458
First Author: M. Sarzi
Corr. Author: M. Sarzi

INSTRUCTIONS

We encourage you to use Adobe's editing tools (please see the next page for instructions). If this is not possible, please list clearly in an e-mail. Please do not send corrections as track changed Word documents.

Changes should be corrections of typographical errors only. Changes that contradict journal style will not be made.

These proofs are for checking purposes only. They should not be considered as final publication format. The proof must not be used for any other purpose. In particular we request that you: do not post them on your personal/institutional web site, and do not print and distribute multiple copies. Neither excerpts nor all of the article should be included in other publications written or edited by yourself until the final version has been published and the full citation details are available. You will be sent these when the article is published.

1. **Licence to Publish:** Oxford Journals requires your agreement before publishing your article. If you haven't already completed this, please sign in with your My Account information and complete the online licence form. Details on how to do this can be found in the Welcome to Oxford Journals email.
2. **Permissions: Permission to reproduce any third party material in your paper should have been obtained prior to acceptance. If your paper contains figures or text that require permission to reproduce, please inform me immediately by email.**
3. **Author groups:** Please check that all names have been spelled correctly and appear in the correct order. Please also check that all initials are present. Please check that the author surnames (family name) have been correctly identified by a pink background. If this is incorrect, please identify the full surname of the relevant authors. Occasionally, the distinction between surnames and forenames can be ambiguous, and this is to ensure that the authors' full surnames and forenames are tagged correctly, for accurate indexing online.
4. **Figures:** If applicable, figures have been placed as close as possible to their first citation. Please check that they are complete and that the correct figure legend is present. Figures in the proof are low resolution versions that will be replaced with high resolution versions when the journal is printed.
5. **Missing elements:** Please check that the text is complete and that all figures, tables and their legends are included.
6. **Special characters and equations:** Please check that special characters, equations and units have been reproduced accurately.
7. **URLs:** Please check that all web addresses cited in the text, footnotes and reference list are up-to-date.
8. **Funding:** If applicable, any funding used while completing this work should be highlighted in the Acknowledgements section. Please ensure that you use the full official name of the funding body.

AUTHOR QUERIES - TO BE ANSWERED BY THE CORRESPONDING AUTHOR

The following queries have arisen during the typesetting of your manuscript. Please answer these queries by marking the required corrections at the appropriate point in the text.

Query No.	Nature of Query	Author's Response
Q1	Author: The figures have been processed according to information entered by you during the submission of your manuscript. If you have already requested print colour figures or have now decided to have print colour figures please confirm that you are willing to pay the £200 (+VAT) charge. You will be invoiced upon publication. Black and white versions of figures are provided at the end of the paper. Please check the black and white versions to assess their quality for the print version of the journal, and contact us if you have any concerns.	OK
Q2	Author: Please supply email addresses for between one and three authors who are willing to correspond with readers and for their email address to be included in the article	m.sarzi@herts.ac.uk, lcoccato@eso.org, enricomaria.corsini@unipd.it
Q3	Author: To check that we have your surnames correctly identified and tagged (e.g. for indexing), we have coloured pink the names that we have assumed are surnames. If any of these are wrong, please let us know so that we can amend the tagging.	OK
Q4	Author: If you refer to any data bases in your paper, please note the journal policy for properly crediting those responsible for compiling the data base. Rather than citing only a URL, if at all possible please also cite a reference (and include it in the reference list), or if a reference is not available then the names of those who compiled the data base. Note that some data bases do provide guidelines on how they should be cited – please check for these and follow them in your paper where appropriate.	OK
Q5	Author: Please note that it is journal style to refer to 'our' Galaxy with a capital 'G' (e.g. in case of Galaxy, Galactic Centre or Galactocentric) and to other galaxies with a lowercase 'g'. Please check that all the notations in this paper are correct.	OK
Q6	Author: The MNRAS list of approved key words has been revised and updated. The new list is appended to these proofs. If you had previously selected key words from the old list, please now check them carefully against the new list in case they need to be changed, or there are new ones that you would like to add. If you had not previously selected key words from the MNRAS approved list, please now choose up to six from the new list.	OK
Q7	Author: Please note that it is journal style to refer to 'our' Galaxy with a capital 'G' (e.g. in case of Galaxy, Galactic Centre or Galactocentric) and to other galaxies with a lowercase 'g'. Please check that all the notations in this paper are correct.	OK
Q8	Author: Please check the figures in the PDF proof carefully.	OK
Q9	Author: As per journal style, the running head short title of a paper must not exceed 45 characters (including spaces between words and punctuation marks); please supply an alternative short title of up to 45 characters (including any spaces between words and punctuation marks) that can be used instead.	The suggested short title "The nuclear disk of NGC4458" is fine by me

Query No.	Nature of Query	Author's Response
Q10	Author: Please note that computer software/programming languages must be styled in SMALL CAPITAL LETTERS, according to journal style. Please check and correct this paper accordingly.	OK
Q11	Author: 'NDSs' has been changed to 'NSDs' here. Please check for correctness.	OK
Q12	Author: Are there any acknowledgements that you would like to add?	Yes, please add: "We are grateful to the anonymous referee for carefully reading our manuscript and for providing comments that helped improving this work."
Q13	Author: Please update this reference, if possible, with full details to be added to the references list.	This is now: Coccato L. et al. A&A, 581, A65
Q14	Author: Please update this reference, if possible, with full details to be added to the references list.	This paper has been accepted for publication on MNRAS and its proof have just been processed, so please double-check your records to find its planned volume and page.
Q15	Author: Please update this reference, if possible, with full details to be added to the references list.	This is now: Sarzi M, Ledo H. R.. Dotti, 2015, MNRAS, 453, 1070

MAKING CORRECTIONS TO YOUR PROOF

These instructions show you how to mark changes or add notes to the document using the Adobe Acrobat Professional version 7 (or onwards) or Adobe Reader X (or onwards). To check what version you are using go to **Help** then **About**.
The latest version of Adobe Reader is available for free from get.adobe.com/reader.

Displaying the toolbars

Adobe Professional X, XI and Reader X, XI

Select **Comment, Annotations and Drawing Markups.**
If this option is not available, please let me know so that I can enable it for you.

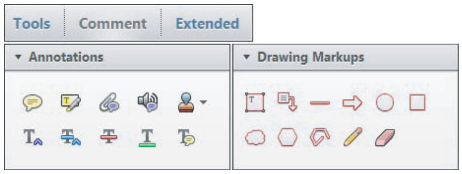

Acrobat Professional 7, 8 and 9

Select **Tools, Commenting, Show Commenting Toolbar**.

Using Text Edits

This is the quickest, simplest and easiest method both to make corrections, and for your corrections to be transferred and checked.

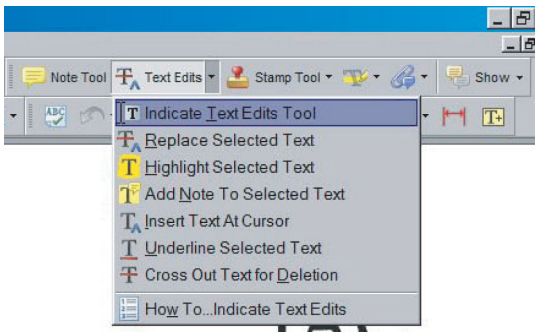

1. Click **Text Edits**
2. Select the text to be annotated or place your cursor at the insertion point.
3. Click the **Text Edits** drop down arrow and select the required action.

You can also right click on selected text for a range of commenting options.

Pop up Notes

With *Text Edits* and other markup, it is possible to add notes. In some cases (e.g. inserting or replacing text), a pop-up note is displayed automatically.

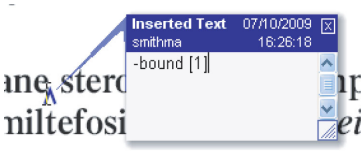

To **display** the pop-up note for other markup, right click on the annotation on the document and selecting **Open Pop-Up Note**.

To **move** a note, click and drag on the title area.

To **resize** of the note, click and drag on the bottom right corner.

To **close** the note, click on the cross in the top right hand corner.

To **delete** an edit, right click on it and select **Delete**. The edit and associated note will be removed.

SAVING COMMENTS

In order to save your comments and notes, you need to save the file (**File, Save**) when you close the document.
A full list of the comments and edits you have made can be viewed by clicking on the Comments tab in the bottom-left-hand corner of the PDF.

Nuclear discs as clocks for the assembly history of early-type galaxies: the case of NGC 4458

M. Sarzi,[1⋆] H. R. Ledo,[1] L. Coccato,[2] E. M. Corsini,[3,4] M. Dotti,[5,6] S. Khochfar,[7] C. Maraston,[8] L. Morelli[3,4] and A. Pizzella[3,4]

[1]*Centre for Astrophysics Research, University of Hertfordshire, College Lane, Hatfield AL10 9AB, UK*
[2]*ESO, Karl-Schwarzschild-Strasse 2, D-85748 Garching, Germany*
[3]*Dipartimento di Fisica e Astronomia 'G. Galilei', Università di Padova, vicolo dell'Osservatorio 3, I-35122 Padova, Italy*
[4]*INAF-Osservatorio Astronomico di Padova, vicolo dell'Osservatorio 5, I-35122 Padova, Italy*
[5]*Dipartimento di Fisica G. Occhialini, Università degli Studi di Milano, Bicocca, Piazza della Scienza 3, I-20126 Milano, Italy*
[6]*INFN, Sezione di Milano-Bicocca, Piazza della Scienza 3, I-20126 Milano, Italy*
[7]*Institute for Astronomy, University of Edinburgh, Royal Observatory, Blackford Hill, Edinburgh EH9 3HJ, UK*
[8]*Institute of Cosmology and Gravitation, University of Portsmouth, Dennis Sciama Building, Portsmouth PO1 3FX, UK*

Accepted 2016 January 11. Received 2015 December 21; in original form 2015 July 15

ABSTRACT

Approximately 20 per cent of early-type galaxies host small nuclear stellar discs that are tens to a few hundred parsecs in size. Such discs are expected to be easily disrupted during major galactic encounters, hence their age serve to constrain their assembly history. We use VIsible MultiObject Spectrograph integral-field spectroscopic observations for the *intermediate-mass* E0 galaxy NGC 4458 and age-date its nuclear disc via high-resolution fitting of various model spectra. We find that the nuclear disc is at least 6 Gyr old. A clue to gain narrow limits to the stellar age is our knowledge of the nuclear disc contribution to the central surface brightness. The presence of an old nuclear disc, or the absence of disruptive encounters since $z \sim 0.6$, for a small galaxy such as NGC 4458 which belongs to the Virgo cluster, may be consistent with a hierarchical picture for galaxy formation where the smallest galaxies assembles earlier and the crowded galactic environments reduce the incidence of galaxy mergers. On the other hand, NGC 4458 displays little or no bulk rotation except for a central kpc-scale kinematically decoupled core. Slow rotation and decoupled core are usually explained in terms of mergers. The presence and age of the nuclear disc constraint these mergers to have happened at high redshift.

Key words: galaxies: elliptical and lenticular, cD – galaxies: evolution – galaxies: formation – galaxies: nuclei – galaxies: structure.

1 INTRODUCTION

In the context of a dark-matter dominated Universe galaxies should have grown through a combination of star formation and merging processes, whereby on the one hand star formation was regulated by the presence of fresh gaseous material and the negative feedback of supernovae and possibly also active nuclei, and on the other hand merging events should have proceeded in a hierarchical fashion. A steady increase in the quality and scope of spectroscopic investigations of nearby galaxies has allowed us to constrain directly their star formation history (e.g. Thomas et al. 2005, 2010, for early-type galaxies), but reconstructing the assembly history of galaxies has proved so far to be more difficult. Attempts to quantify the rate of merging events by searching close galactic pairs and interacting galaxies (e.g. Darg et al. 2010) depend on the depth and the area covered by the images used in these studies, whereas individual investigations of morphological signatures of past mergers, such as galaxy shells, can hardly pinpoint the epoch of such a galactic encounter (but see Hau, Carter & Balcells 1999). The lack of constraints on the assembly history of nearby galaxies leaves unchecked several predictions of the hierarchical standard paradigm. For instance, the most massive galaxies should have assembled only recently (e.g. De Lucia et al. 2006; Khochfar & Silk 2006) whereas, at a given mass, galaxies in clusters should have experienced less merging events than their counterparts in the field since when they entered such crowded galactic environments. Indeed in clusters galaxies fly too fast by each other to merge efficiently.

Understanding the assembly history of galaxies is particularly important in the case of early-type galaxies, as these systems have long

⋆ E-mail: m.sarzi@herts.ac.uk

been thought to originate during merging events (Toomre 1977). In fact, the kinematic distinction between fast and slowly rotating early-type galaxies, first suggested with long-slit data (e.g. Illingworth 1977; Binney 1978; Davies et al. 1983; Bender, Saglia & Gerhard 1994) and recently quantified thanks to integral-field data (Cappellari et al. 2007; Emsellem et al. 2007) is suggestive also of a separate merging history for these two kinds of objects (Emsellem et al. 2011; Khochfar et al. 2011; Naab et al. 2014), where slow rotators would owe their low angular momentum to a more systematic bombardment by smaller satellite galaxies.

In this respect, nuclear stellar discs (NSDs) could prove important tools to directly constrain the assembly history of early-type galaxies. Initially discovered in images taken with the *Hubble Space Telescope* (*HST*; van den Bosch et al. 1994) and now known to be common in early-type galaxies (in up to 20 per cent of them Ledo et al. 2010), such small discs (a few ∼100 pc in radius at most) are indeed fragile structures that should not survive a significant merger event (see, e.g. the simulations shown in Sarzi, Ledo & Dotti 2015). This means that by dating the stellar age of the NSDs, it is possible to place a lower limit for the look-back time since their host galaxies experienced a major encounter, as NSDs could form also after such an event. In fact, the stellar age of NSDs can be constrained even more precisely than is generally the case for other kinds of galactic component, thanks to the possibility to derive in advance their relative contribution to the total galaxy light.

The main difficulty in disentangling a superposition of two stellar populations in the spectra of a galaxy, in this case the nuclear disc and the bulge, is the degeneracy between the age and light fractions of each component. Using good quality and extended spectra allows us to better exploit the information encoded in the stellar absorption lines and can help mitigating this problem, but in the presence of relatively old stellar populations further complications arise from the degeneracy between age and metallicity or reddening. On the other hand, in the case of structurally different and, to some extent, well described, galactic components it may be possible to infer from images their individual light fractions in the considered spectra (in the wavelength range covered by the images), and exploit this constrain to break the previous degeneracies. This is precisely the case of a nuclear disc embedded in a stellar bulge, where the surface brightness distribution of the disc can be inferred using the disc–bulge decomposition technique introduced by Scorza & Bender (1995), which relies only on the assumption of an exponential radial profile for the disc and an elliptical shape for the bulge isophotes (see also, e.g. Pizzella et al. 2002; Morelli et al. 2004, 2010; Corsini et al. 2012).

Simple simulations such as those shown in Fig. 1 serve to illustrate the dramatic effect that an a priori knowledge of the disc-light contribution should have in estimating the age of NSD embedded in a bulge. Fig. 1 shows the case of a 7-Gyr-old disc population embedded in a 13-Gyr-old bulge, where both components contribute to the input model spectrum with the same broad-band flux in the 4500–5500 Å range and are represented by single-age stellar population models of solar metallicity (from Maraston & Strömbäck 2011). When trying to match different noisy realizations of such input model by combining the correct bulge template (as if the bulge stellar properties had also been previously constrained) with disc model populations of varying age and metallicity, the χ^2 contours around the input disc stellar age of 7 Gyr increase steeply to high values if the relative contribution of the bulge and disc component are fixed to their input value (as if they were known from a disc–bulge decomposition, Fig. 1 right-hand panel). On the

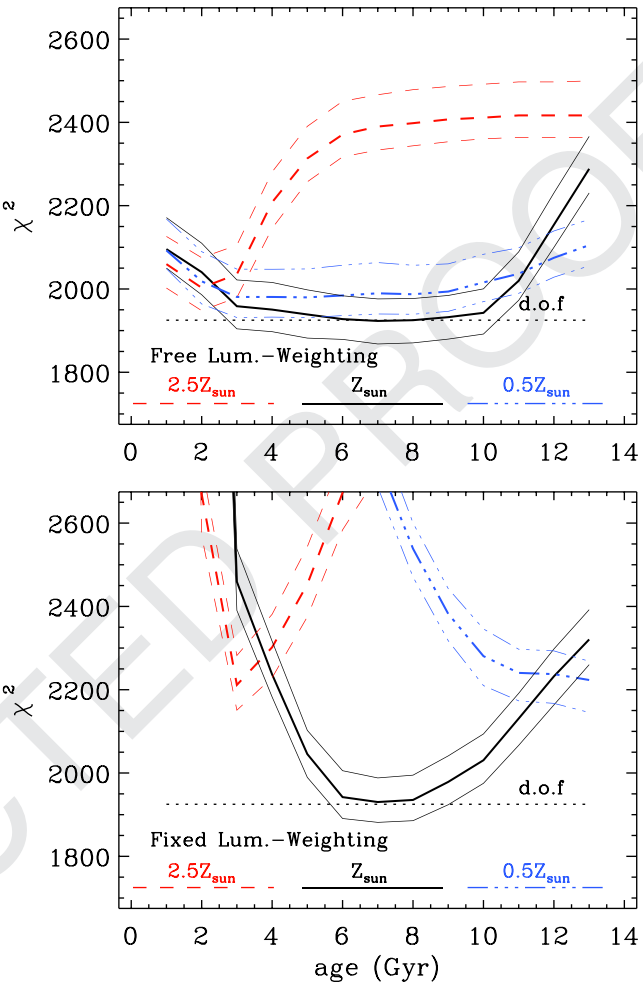

Figure 1. Simulations showing the accuracy in recovering the age of a 7-Gyr-old disc population that is embedded in a 13-Gyr-old bulge population. The bulge and disc populations contribute with the same broad-band flux between 4500 and 5500 Å to the input model, and are represented by single-age stellar population models of solar metallicity from Maraston & Strömbäck (2011), covering the entire wavelength range of our VIMOS observations (Section 3). Different amounts of kinematical broadening were also included in the bulge and disc models ($\sigma = 200$ and 100 km s^{-1}), and statistical fluctuations were added to simulate an S/N ∼ 100. In both panels, the thick solid line shows the average quality of the fit to the input model as disc single-age models of increasing ages are combined with the right, 13-Gyr-old, bulge population model, which mimics the situation where the bulge stellar properties have been previously constrained from off-centred observations. The thin solid lines indicate the 1σ fluctuation that is derived by fitting different realizations of the input model. The dashed and dot–dashed lines show the quality of the fits obtained while considering disc populations of supersolar and subsolar metallicities. On the left-hand panel, the relative contribution to the fit of the bulge and disc populations is left free to vary, whereas on the right-hand panel each component is constrained to contribute the same broad-band flux in the 4500–5500 Å range as in the input model. In both cases, the kinematic broadening of the templates is also freely adjusted during the fit. The comparison between χ^2 curves in the left- and right-hand panels illustrates how knowing in advance the disc-light contribution allows one to recover the correct disc age and metallicity, whereas without such an initial clue estimating the disc age and metallicity would be complicated by the well-known degeneracy between these two parameters.

other hand, when the relative contribution of the disc and bulge templates are not constrained, it is possible to obtain a very good match to the input spectrum also when using disc populations of considerably different age and metallicity than the input that of the input disc template (Fig. 1, left-hand panel). In other words, this experiment shows that knowing in advance the disc-light contribution should allow estimating more robustly the NSD age and metallicity.

Motivated by the potential use of NSDs as clocks for the assembly history of their host galaxies and encouraged by the previous kind of simulations, this paper presents a pilot investigation based on integral-field spectroscopic observations of the NSD in the Virgo elliptical galaxy NGC 4458, which has a well-known nuclear disc (Morelli et al. 2004, 2010) and thus constitutes an ideal laboratory for testing how accurately we can estimate the age of NSDs. This paper is organized as follows. In Section 2, we describe our observations with the Very Large Telescope (VLT) and the reduction of our data taken with the VIsible MultiObject Spectrograph (VIMOS). The core of our analysis is found in Section 3, where start by estimating the relative contribution of the bulge and NSD light in our central VIMOS spectra (Section 3.1), extract a template for stellar bulge population (Section 3.2) and finally constrain the stellar age of the nuclear disc (Section 3.3). Finally, in Section 4 we discuss our results, suggesting also some future avenues for the methodology developed here (Section 4.2).

2 VIMOS OBSERVATIONS AND DATA REDUCTION

2.1 Observations

The VIMOS integral field unit (IFU; Le Fèvre et al. 2003), installed on the Melipal-UT3 of the VLT, presented itself as one of the best instruments for this study. With VIMOS, it is indeed possible to extract spectra of intermediate spectral resolution over a relatively long wavelength range and at different spatial locations, which allows us to study the stellar population of NSDs while constraining also the properties of the surrounding stellar bulge. Yet, it is the large collecting power of VLT and the possibility to obtain observations under the best seeing conditions that make VIMOS ideal to study NSDs, as these contribute significantly to the total stellar light only over very small spatial scales.

The VIMOS data for NGC 4458 were collected in service mode on 2007 April (P79) and between 2008 April and June (P81), using the HR blue grating with no filter and while opting for highest spatial magnification. Such a configuration lead to data cubes comprising of 1600 spectra extending from 4150 to 6200 Å and with spectral resolution of 2 Å (FWHM), each sampling an area 0.33 arcsec × 0.33 arcsec within a total field of view of 13.0 arcsec × 13.0 arcsec. To allow for a proper sky subtraction and minimize the impact, the dead fibres or pixels, each observing block consisted of two, slightly offset on-source pointing (each 940 s long in P79 and 1025 s in P81), bracketing a shorter sky exposure (for 480 s and 500 s in P79 and P81, respectively). Out of a total allocated time of 23 h, considering that only one observing block was executed in P79, this strategy yielded a total of 5.7 h on target. All these observations were taken under very good atmospheric seeing conditions, on average around 0.8 arcsec, and at an average airmass of ∼1.33.

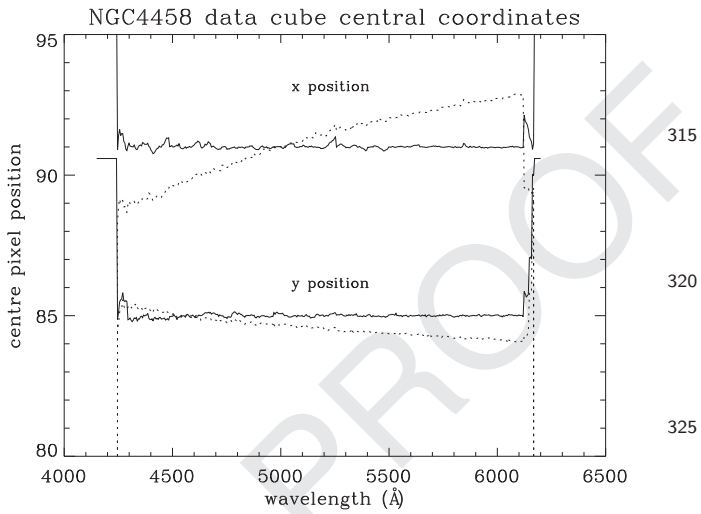

Figure 2. The *x* and *y* centre coordinates of NGC 4458 as a function of wavelength along the VIMOS data cube before (dotted lines) and after our extra rectification (solid lines).

2.2 Data reduction

We started the reduction of our data by running each of our single sky and on-target exposures through the VIMOS ESO pipeline,[1] thus carrying out the bias subtraction, flat-fielding, fibre identification and tracing, and wavelength calibration. We then used in-house IDL and IRAF procedures to further correct for the different relative transmission of the VIMOS quadrants, which we adjusted by requiring the same intensity for the night-sky lines across the field of view, and in order to subtract the sky spectrum from the galaxy pointings. During this last step, we compensate for time variations in the night sky spectrum between the on-target and sky pointing by adjusting the strength of the strongest night sky lines in the sky exposures to match what found in the galaxy pointings. Finally, each on-target exposure was organized in data cubes using the tabulated position in the field of view of each fibre, which were then merged in a final data cube by aligning the bright nuclear regions of NGC 4458 in the total reconstructed images corresponding to each single cube.

Although these steps should have sufficed in providing a fully reduced data cube, we noticed that an extra rectification was needed to account for a residual systematic shift of the galaxy centre as we move along the wavelength direction in the data cube. Such a shift is likely due to atmospheric differential refraction, as the galaxy centre moves mostly along the *x*-axis of our data cube and that this is close to north–south direction. Fortunately, the nuclear regions of NGC 4458 are sufficiently cuspy for us to accurately locate the galaxy centre as a function of wavelength, thus correcting for this systematic shift. Fig. 2 shows the galaxy centre *x* and *y* pixel coordinates as a function of wavelength, before and after rectifying our final data cube. Even though the centre of NGC 4458 moved only by 1.5 arcsec between the blue and red ends of our data cube, correcting for this shift is particularly important in the context of this work, since the NSD of this galaxy contributes significantly to the central light distribution only within a few tens of an arcsecond (see Morelli et al. 2004). In fact, ensuring an accurate rectification meant restricting the final wavelength range of our data cube between 4220 and 6000 Å. The final quality of our data can be appreciated

[1] version 2.2.1 http://www.eso.org/sci/software/pipelines/.

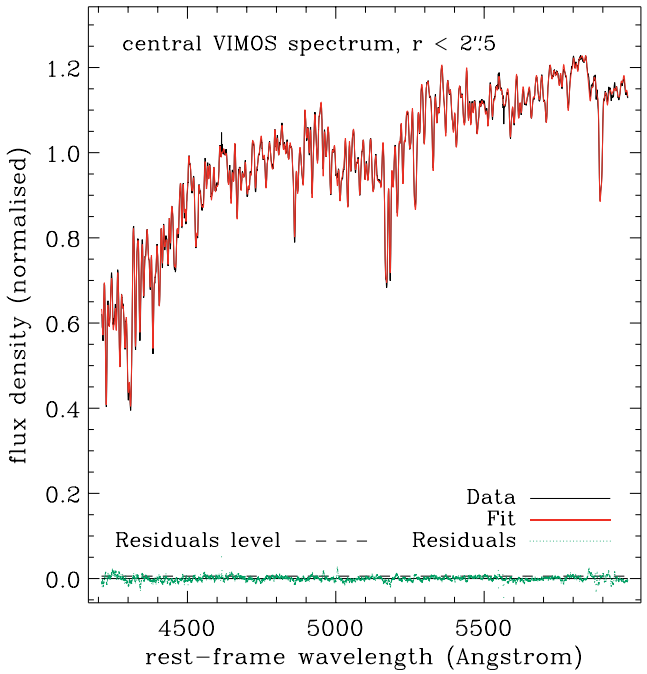

Figure 3. Central 5 arcsec VIMOS spectrum of NGC 4458 and our best pPXF fit using the entire MILES spectral library. The level of fluctuations in the residuals of this fit correspond to an average value of 175 for the signal over residual-noise ratio.

in Fig. 3, where we show the integrated spectrum of NGC 4458 within the central 5 arcsec. Based on the residuals of the best-fitting model for the stellar spectrum, obtained the pixel-fitting code of Cappellari & Emsellem (2004, pPXF) and the whole MILES stellar library (Sánchez-Blázquez et al. 2006), we obtain an average value of 175 for the signal over residual-noise ratio. For comparison, within a similar aperture and for 2 h of on-source exposure time, the SAURON integral-field data for NGC 4458, first presented by Emsellem et al. (2004), come with a signal over residual-noise ratio ∼250 in the 4850–5300 Å wavelength region.

3 ANALYSIS

As we covered in the introduction, in order to best estimate the stellar age of the nuclear disc in NGC 4458 we ought to know the relative contribution of the disc and its surrounding bulge to the central stellar surface brightness distribution, preferably within a wavelength range that is covered by our spectra. For this, we will use the results of the disc–bulge decomposition of Morelli et al. (2004), which was based on *HST*-*F*555*W* images in the visible domain, and by accounting for the difference in spatial resolution and spatial sampling between *HST* and VIMOS we will estimate the disc contribution to each of our central VIMOS spectra (Section 3.1). Thanks to the integral-field nature of our data, we will then extract a central aperture spectrum while striking a good compromise between signal-to-noise ratio and disc-light contribution, as well as an off-centred aperture spectrum dominated by the bulge light that could be used as a template for such a component (Section 3.2) in our final stellar-population analysis of the nuclear regions (Section 3.3).

3.1 *HST* to VIMOS matching

Starting from the disc–bulge decomposition of Morelli et al. (2004), we can account for the lower spatial (seeing-limited) resolution and the coarser spatial sampling of the VIMOS observations to compute the fraction of disc-light that would have been observed within each VIMOS resolution element, if using the same filter of the *HST* images. We started such a matching procedure by rotating the *HST* image of NGC 4458 to match the orientation of the VIMOS reconstructed image. Then, after extracting only its central regions, we proceeded to convolve the *HST* image by a double-Gaussian meant to represent the atmospheric point spread function (PSF) of VIMOS and finally resampled the resulting degraded image within the 0.33 arcsec× 0.33 arcsec VIMOS spaxels. To match the VIMOS reconstructed image, this procedure required a rather vertically elongated PSF, which effectively greatly reduces our spatial resolution in that direction. This problem is only briefly mentioned in the VIMOS documentation and would appear to be due to the placing of the IFU unit at the edge of the VIMOS field of view (Anguita et al. 2008). On the other hand, the extent of the PSF along the horizontal direction would appear to remain at the nominal level we requested (of 0.8 arcsec, Section 2).

Fig. 4 helps assessing the accuracy of our *HST* to VIMOS matching, and further shows the final map for the values of the disc-to-total ratio in the VIMOS resolution elements. The latter was obtained by simply applying the same rotation, convolution and resampling steps (using the previously derived best double-Gaussian PSF) to the best-fitting disc model image that was derived by Morelli et al. (2004), and by then dividing the result by the degraded *HST* image of NGC 4458. Such a disc-to-total ratio map shows that in the central VIMOS spectra, we can expect a disc contribution nearly up to 5 per cent.

3.2 Bulge spectrum analysis

To better constrain the age of the NSD in the central region where its light contribution is the greatest, we ought to also have the best possible model for the bulge stellar spectrum, which will none the less dominate the central spectrum we are about to analyse. For this, we combined two bulge spectra extracted within two 3×3 pixels apertures in opposite directions 2.5 arcsec away from the centre along the major axis of NGC 4458 (that is, horizontally in Fig. 4). Since we aim to reduce the impact of stellar population gradients in the bulge, these are indeed the closest regions to the centre where the contribution of the nuclear disc is negligible, well below 1 per cent, the level at 2 arcsec, as can be seen on the lower-right panel of Fig. 4. Were it not for the peculiar vertically elongated character of the VIMOS PSF, we would have extracted our bulge aperture spectrum along the minor axis.

Following the extraction of such a representative bulge spectrum, we proceeded to match it in the best possible way using pPXF and the entire MILES stellar library. Using all the 985 stellar spectra in the MILES library allowed us to match also those spectral features that are notably hard to reproduce when using stellar population synthesis models owing to abundance patterns that can only be partially accounted for in these templates (e.g. the Mgb region; see also Sarzi et al. 2010). In this fit, we allowed for interstellar extinction (adopting a Calzetti et al. 2000 reddening law) and for an additional fourth-order additive polynomial correction of the stellar continuum. The weights assigned to each MILES template during the pPXF fit were then used to construct an optimal template for the bulge stellar population.

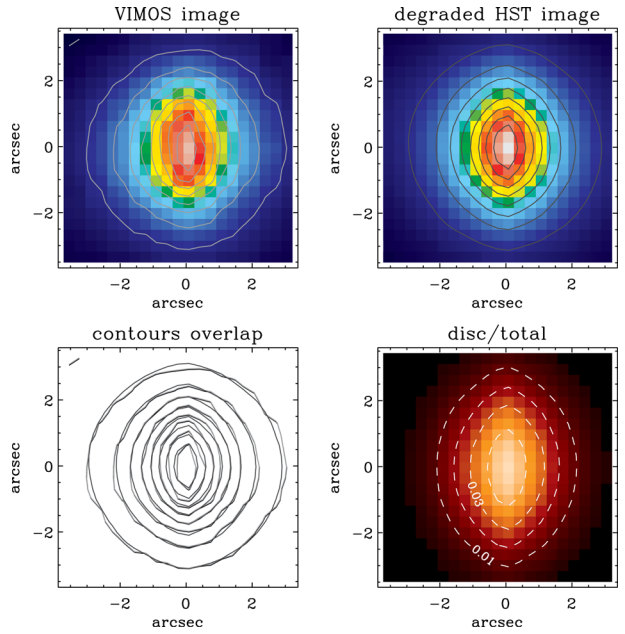

Figure 4. Upper panels: central parts of the VIMOS reconstructed image of NGC 4458 (left) and the same for the *F*555*W* Wide Field Planetary Camera 2 image, once degraded to match the spatial resolution of VIMOS and resampled within the 0.33 arcsec× 0.33 arcsec resolution elements of the high-resolution configuration of VIMOS (right). Lower left: overlap of the surface brightness contours for the VIMOS and degraded *HST* image (in light and dark grey lines, respectively), which are also shown in the corresponding upper panels. Lower right: map for the disc-to-total light ratio computed from the *HST* degraded image shown in the upper-right panel and a similarly convolved and resampled version for the image of the best-fitting disc model that was obtained during the Scorza & Bender disc–bulge decomposition of Morelli et al. (2004). The dashed contours on this last image show the level of disc-light contribution in the VIMOS spaxels (but see the text). Note that the major axis of NGC 4458 and its nuclear disc runs nearly parallel to the *x*-axis of the VIMOS cube, and the vertical elongation shown here is the results of the rather elongated point-spread function of VIMOS and the steep profile of the intrinsic surface brightness of this galaxy.

3.3 Nuclear stellar population analysis

To estimate the age of the nuclear disc in NGC 4458, we extracted a 3×1 pixels central aperture along the minor axis (that is, vertically in Fig. 4) where the disc-light contribution (in the *F*555*W* filter wavelength region) amounts to ∼5 per cent and the S/N per pixel reaches values of 120. We then used pPXF to fit such a nuclear spectrum with the our bulge template and the single-age stellar population models from both the Maraston & Strömbäck (2011) and Vazdekis et al. (2010) libraries (both based on the MILES spectral atlas) in order to represent the disc, which we indeed assume to have formed very quickly. We constrained the age of the nuclear disc by considering, at a given stellar metallicity, each one of the population models for the disc at a time, combining them with our empirical bulge template in two different ways. In the first approach (the free fit), we allow pPXF to choose freely the relative weight of these two templates, whereas in the second (the constrained fit) we accounted for the relative light contribution that bulge and disc templates should contribute to the nuclear spectrum, that is 95 and 5 per cent for the bulge and disc, respectively. More specifically, since the disc-light contribution within our central VIMOS aperture that we derived in Section 3.1 refers to the light fraction in the same band-pass of the *HST* images for NGC 4458, prior to our pPXF fit

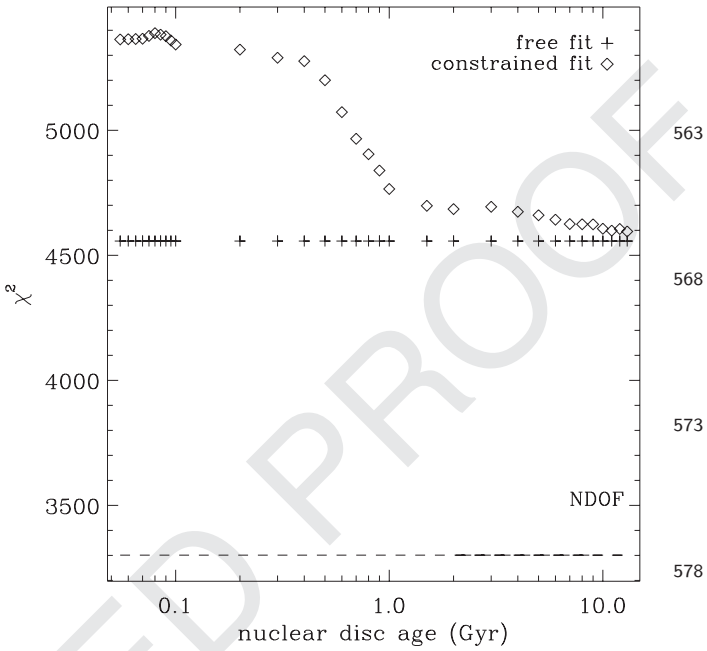

Figure 5. Quality of our constrained (diamonds) and free (plus signs) fits as a function of the stellar age of the NSD, or more specifically, of the single-age stellar population model for disc that is combined with our empirical bulge template. Even though the quality of these fits is relatively poor compared to the quality of the fit that can be achieved through a free combination of all the stellar templates in the MILES library (as done for the bulge spectrum in Section 3.2, horizontal dashed line), the observed trends for our constrained indicates a very old stellar age for the nuclear disc. In fact, this is also the case of the free fit, since only the bulge template is used. All χ^2 values were computed after rescaling the formal uncertainties on the flux densities of our nuclear spectrum so that the best fit based on the entire MILES stellar library (Section 3.3) sets our standard for a good fit, thus making the corresponding χ^2=NDOF.

we integrated the flux of our templates within the *F*555*W* passband (accounting for the fact that the *F*555*W* filter response tails off to longer wavelength than the VIMOS data), and then used such integrated fluxes when weighting them during the constrained fit. During this preliminary step, we also reddened each of the model templates and the bulge template by our best measurement of the interstellar extinction towards the nucleus. This reddening estimate was obtained by performing a pPXF fit to the nuclear spectrum using the entire MILES stellar library as done previously for the bulge aperture, a fit that will also set the standard for the best possible model for our nuclear spectrum.

Using first the Maraston & Strömbäck models, Fig. 5 shows the results of this exercise, where the quality of the pPXF fit in the free and constrained cases are compared as a function of stellar-population age for the disc template, in this case, of Solar metallicity. In both instances, the formal uncertainties in the flux-density values of the nuclear spectra where rescaled in order for our best possible fit, the one obtained using the entire MILES library, to have χ^2 value equal to the number of degree of freedom of our fit (NDOF). Both free and constrained approaches indicate that the nuclear disc must indeed be very old, possibly as old as the bulge. The free pPXF fit indeed always prefer to use only our bulge template, which is itself best fitted using the oldest and slightly metal-poor (half solar) of our single-age templates (consistent with the results of both Morelli et al. 2004; Kuntschner et al. 2010), whereas during the constrain approach only the oldest disc templates lead to similarly good fits.

The behaviour of the free and constrained fits in Fig. 5 is more dramatic than that shown in our initial simulations, and is due to the presence of an overabundance pattern in alpha elements in our nuclear data, in particular in the spectral region corresponding to the Mgb Lick index (González 1993). This abundance pattern is partially accounted for by our empirical bulge template, and the fit in these regions is only made worse during the constrained fit where the quality of the fit quickly deteriorates as we force the use of a progressively younger disc template that contributes to ∼5 per cent of the light in the nuclear spectrum (as expected from the disc–bulge decomposition of Morelli et al. 2004).

In Fig. 5, our rescaling of the formal uncertainties on the flux density in our spectra is useful to show that our models for estimating the age of the disc cannot quite match the quality of a fit that allows for any possible mix (even unphysical ones) of stellar spectra entering our nuclear spectrum of NGC 4458. In fact, even when adopting such an empirical description for the bulge, the use of our empirical template, with or without the addition single-age stellar population models for the disc, we obtain fits that are $\gtrsim$40 per cent worse than our best fit. This may highlight the presence of a substantial central gradients in the properties of the bulge populations that we cannot capture with our bulge template, limitations in the spectral synthesis models that we adopt for the disc, or that the disc formation was instead rather prolonged. Given that our tools of trade are not optimal, in order to be as conservative as possible in placing a lower limit on the age of the disc based on $\Delta\chi^2$ statistics, we ought to further artificially broaden our flux-density errors until our best constrained pPXF fit becomes formally a good fit (i.e. until the corresponding χ^2 reaches down to NDOF). In fact, for our final estimate of the disc age, we decided to further restrict our analysis to the spectral regions around the age-sensitive Hδ and Hβ stellar absorption features. This does not bring much loss of information, since most of the difference between our models occur in these spectral regions (from 90 to 40 per cent of the quadratic difference when comparing models including young and old disc models or for old disc ages only, respectively; see also Fig. 6), and has the advantage of making our age estimates less sensitive to the way the polynomials adjust the continuum shape of our models, on which we have little control during the pPXF fit. Finally, we considered single-age stellar population models for the nuclear disc of half and twice solar metallicity, in addition to the solar metallicity models used in our first attempt of Fig. 5.

Fig. 7 shows the run of the quality of our constrained fit in the Hδ and Hβ spectral windows as a function of the age of the disc population model that is combined with our empirical bulge template, with different lines indicating the use of single-age models of different stellar metallicity. As anticipated above, all formal uncertainties on the flux-density values of our nuclear spectra have been rescaled until our best constrained pPXF fit – in this case including a stellar disc of super-Solar metallicity – lead to a χ^2 value equal to NDOF across the entire wavelength range. The χ^2 values plotted in Fig. 7 correspond then only to the portion of our spectra within 30 Å of the Hδ and Hβ absorption lines at 4340 and 4861 Å, respectively. Setting a one-parameter $\Delta\chi^2 = 9$ bar above the χ^2 value of our best-fitting constrained model allows us to finally place a 3σ lower limit of ∼5–6 Gyr on the stellar age of the nuclear disc of NGC 4458. Using the whole spectral range would have yielded a tighter lower limit of ∼7–8 Gyr. We also note that possible nebular in-fill contamination in the Hδ and Hβ spectral regions is excluded as there is little evidence for [O III]λλ4859, 5007emission in the central regions of NGC 4458, either from our data (see Fig. 3) or in the SAURON integral-field data shown by Sarzi et al. (2006).

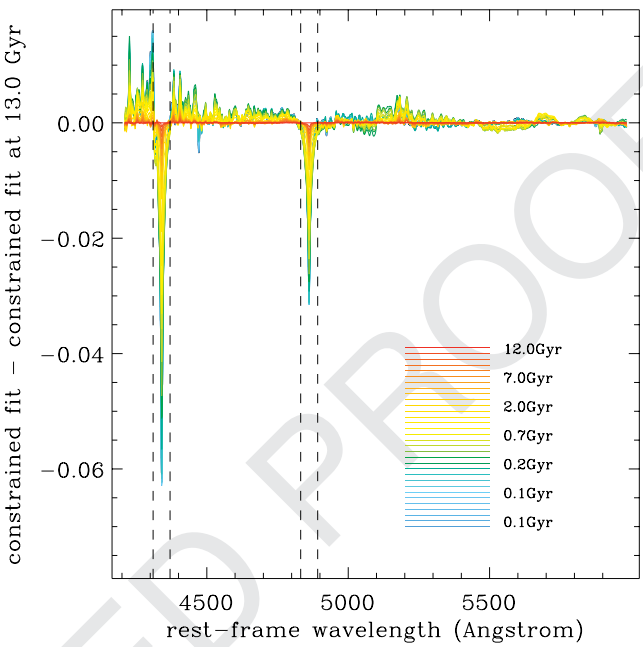

Figure 6. Difference between the best-fitting constrained fit model, which features a 12.6-Gyr-old disc, and all other constrained fits including different single-age disc templates. The largest deviations are observed within the spectral regions identified by the vertical dashed lines, which correspond to the age-sensitive Hδ and Hβ stellar absorption features (at 4340 and 4861 Å, respectively). Nearly 90 per cent of the quadratic difference (relevant for comparing model χ^2 values) with the youngest disc model is contained across these 30 Å-wide spectral windows, with this fraction lowering to ∼40 per cent when comparing our best model with other models featuring old discs.

To conclude, we note that our result do not depend on the choice of stellar population models. For instance, Fig. 8 shows that using the Vazdekis et al. (2010) single-age models for representing the nuclear disc population lead to very similar old age constraints on the disc age. This may have not been the case if the nuclear disc had turned out to be substantially youngers, since model prescription can vary in this case (e.g. Maraston 2005).

4 DISCUSSION

By combining high-quality VIMOS integral-field spectroscopic observations with constraints from *HST* images on the relative contribution of the nuclear disc of NGC 4458 to the central surface brightness of this galaxy we have been able to set a tight limit on the stellar age of such NSD. Our analysis indicates that its formation must have occurred at least ∼5–6 Gyr ago, which in turn suggests that NGC 4458 did not experience any major merger event since that time.

Besides serving as a proof of concept for further measurements in larger samples of NSD-hosting galaxies that could lead to a better understanding of their assembly history, the finding of such an old NSD in NGC 4458 already provides food for thoughts on the formation of the specific class of early-type galaxies that display very little or no bulk rotation. Over the course of the SAURON survey (de Zeeuw et al. 2002) NGC 4458 was in fact classified as one of those so-called slow-rotators (Emsellem et al. 2007), which the ATLAS^{3D} survey (Cappellari et al. 2011) firmly recognized as forming only a minority, ∼14 per cent, of the entire early-type galaxy population (Emsellem et al. 2011). More specifically, NGC

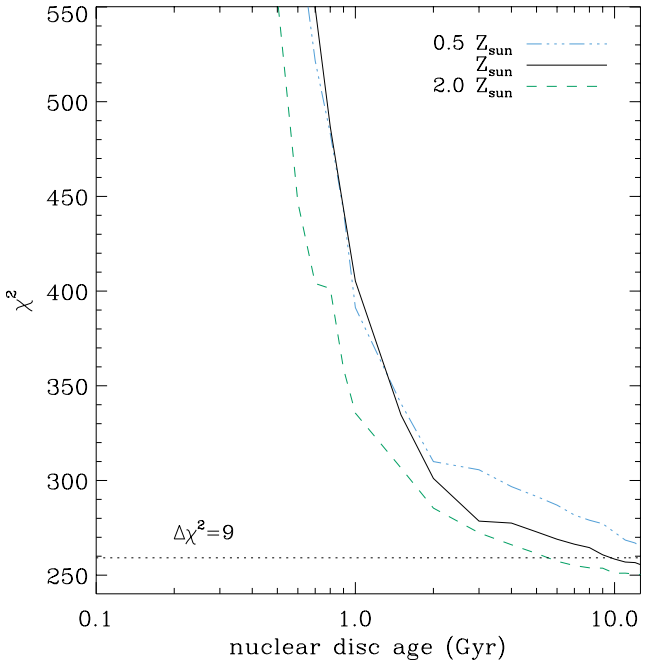

Figure 7. Final stellar age estimate for the NSD of NGC 4458. Similar to Fig. 5, but now based only on constrained fit model featuring single-age disc templates of different metallicities (solid lines for solar values, dot–dashed and dashed for half and twice solar values, respectively) and while assessing the quality of the fits within the Hδ and Hβ spectral windows shown in Fig. 6. All plotted χ^2 values within this spectral region have been computed after rescaling all flux-density errors assuming that the best constrained fit model would yield a χ^2=NDOF across the *entire* spectrum. A $\Delta\chi^2 = 9$ threshold set from the best χ^2 value obtained within the Hδ and Hβ windows indicate that at best, when considering populations of super-Solar metallicity, the nuclear disc could have formed as recently as ∼5–6 Gyr ago.

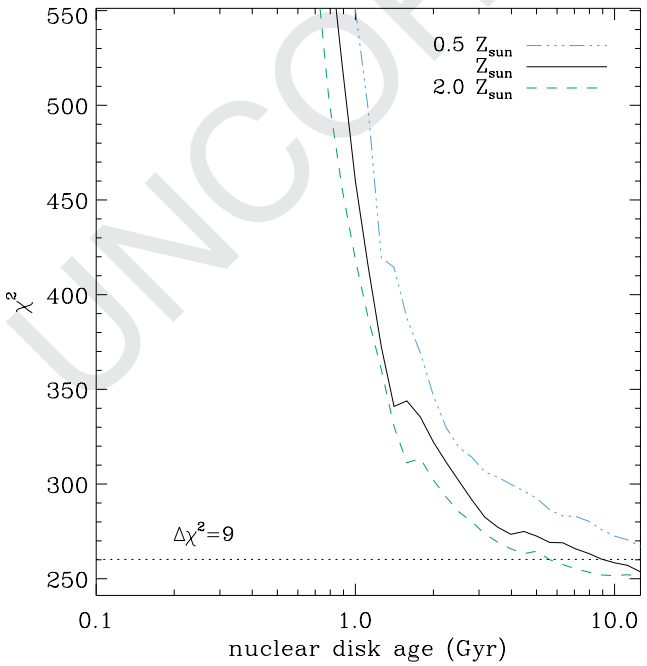

Figure 8. Similar to Fig. 7 but now while adopting the single-age models of Vazdekis et al. (2010), based also on the MILES stellar library.

4458 falls in the kind of slow-rotators that exhibit a central slowly rotating core within a non-rotating main stellar body (also known as a kinematically decoupled core, KDC). As in the case of other galaxies in this class, the kinematic transition to the rotating core (which in the case of NGC 4458 occurs ∼5 arcsec from the centre) does not appear related to any noticeable photometric or stellar-population feature, except that in the case of NGC 4458 an NSD is further found well within it (at 1 arcsec scales).

The formation of slow-rotators is still an open issue for theoretical models. Indeed, whereas from a simple semi-analytical approach the present-day relative fraction of fast and slowly rotating early-type galaxies is well reproduced by considering as fast rotators all objects that in these models have at least 10 per cent of their total stellar mass in a disc component (thanks to a more prolonged gas accretion history; Khochfar et al. 2011), numerical simulations for galaxy interactions still have a hard time reproducing both the kinematic and photometric properties of slow rotators. Under certain conditions binary mergers between discs can lead to remnants resembling slow-rotators with a KDC (Jesseit et al. 2009), but generally such simulated objects are much flatter than real slow-rotators. Additional major merger encounters do not address such a discrepancy, but instead destroy the central core and lead to an overall larger angular momentum (Bois et al. 2011). In fact, it is generally difficult to decrease the stellar angular momentum through major mergers since these encounters bring a great deal of orbital angular momentum that must be conserved (Khochfar & Burkert 2006). For this reason, frequent minor mergers have been advocated as a more efficient means for both removing the angular momentum of galaxies and making them rounder (Khochfar et al. 2011). Yet, even though the negative impact of minor mergers on the angular momentum and flattening has been observed in several numerical simulations carried out in a cosmological context (Naab et al. 2014), there is still limited agreement as regards the intrinsic flattening of simulated and real early-type galaxies (for the latter, see Weijmans et al. 2014, based on the ATLAS^{3D} sample).

In this respect, we note that NGC 4458, with its perfectly edge-on nuclear disc that presumably sits in the equatorial plane, must intrinsically be a nearly spherical galaxy given its apparent axis ratio $b/a = 1 - \epsilon = 0.88$ (where the flattening ϵ is from Emsellem et al. 2011). Furthermore, NGC 4458 is special among slow-rotators, in that it is the least massive object in this class. Its dynamical mass is estimated at $10^{10}\,M_\odot$ (Cappellari et al. 2013), whereas most non-rotators and slow-rotators with a KDC have mass values of $1.8 \times 10^{11}\,M_\odot$ (Emsellem et al. 2011). Both these characteristics make NGC 4458 particularly puzzling. Indeed if the roundness of NGC 4458 could suggest that minor mergers were particularly important in shaping it, its small mass would argue against it since presumably only the most massive systems would have seen many smaller galaxies coming their way during their history. In addition, the odds of NGC 4458 interacting or merging with other galaxies would have further decreased further since it entered the Virgo cluster. The mere presence of an NSD in NGC 4458 could represent an additional argument against a late satellite bombardment (although minor mergers may not always effect the central regions of a galaxy, see Callegari et al. 2009, 2011), whereas the old age of the NSD is consistent with the notion that NGC 4458 did not experience a major merger in a long time and hence had most of its mass in place early-on in its history. Finally, NGC 4458 also hosts a KDC which, as suggested already by many authors for this kind of structures (e.g. Balcells & Quinn 1990; Hernquist & Barnes 1991; Di Matteo et al. 2008; Bois et al. 2011), could have formed during a gas-poor merger event. The presence of an NSD embedded in such a KDC in-

dicates either that the merger event that lead to the formation of the KDC must have preceded the formation of the disc, or alternatively that the nuclear disc could have also formed during such merger thanks to the presence of some gas material. In fact, our analysis also allows for a co-eval formation for the stars encompassed by the nuclear and bulge aperture, which indeed covers the KDC regions.

4.1 Caveats

In our analysis, we have assumed that the NSD of NGC 4458 formed almost instantaneously, although this does not necessarily have to be the case. If the star formation history of the NSD was indeed prolonged this is likely to have been characterized by a number of starbursts each lasting just a few Myr, comparable to the short dynamical time-scales of galactic nuclei and consistent with the finding that central starbursts consume their gas reservoir very efficiently (e.g. Bournaud 2011, and references therein). This is similar to the case of nuclear clusters (Böker et al. 2002, 2004), which display optical spectra that are indeed well matched by a superposition of single-age stellar-population models (Sarzi et al. 2005; Walcher et al. 2005; Rossa et al. 2006). In the case of nuclear clusters, the presence of several stellar subpopulations in nuclear clusters could be investigated only because nuclear clusters are generally young systems, with average ages typically less than a few Gyrs. For the NSD of NGC4458, however, our analysis indicates that the bulk of the stars in the NSD are very old, a result that is robust even when using single-age stellar population models. Indeed, if a significant fraction of young (less than 1–2 Gyr) stars was present in the NSD we would have otherwise inferred a biased luminosity-weighted younger age for it. Given the difficulties in separating old stellar populations from each other, we consider presently unfeasible even with our photometric constraints to disentangle the presence of distinct but similarly old episodes of star formation in the NSD of NGC4458.

4.2 Future outlook

The results of our stellar-population analysis for the central regions of NGC4458 demonstrate the accuracy with which it is possible to constrain the age of NSDs with integral-field data. Considering that such structures are present in up to 20 per cent of early-type galaxies (Ledo et al. 2010) and in few spirals (Pizzella et al. 2002), a similar but systematic investigation of NSDs in galaxies of different mass and across different galactic environments would constitute a promising avenue for constraining the assembly history of early-type galaxies. In fact, Ledo et al. (2010) already provides the most extensive sample of nearby NSDs on which such a follow-up survey could be based, with the recent work of Corsini et al. (2016) already finding an example of a young NSD among the Ledo et al. (2010) sample.

In this respect, the MUSE integral-field spectrograph (Bacon et al. 2010), recently mounted at the Yepun-UT4 of VLT, will be particularly suited for such an NSD census, for several reasons. MUSE is indeed much more efficient than VIMOS (with an overall throughput reaching up to ∼40 per cent) and extends to a longer wavelength range (from 4650 to 9300 Å), allowing a neater separation of the nebular emission from the stellar continuum while retaining a spectral resolution of R ∼3000 sufficient for a detailed estimate of the stellar LOSVD. Finally, and most importantly for the study of NSDs, MUSE will eventually also work with adaptive optics and reach a spatial resolving power comparable to that of *HST*, which will dramatically boost the disc contribution to the nuclear spectra. This will lead to even tighter constraints of the NSD age, in particular if the stellar kinematics observed in the nuclear regions will be also brought in as an additional constraint.

A better NSD-to-bulge contrast and the ability to constrain the stellar LOSVD (in turn thanks to an excellent data quality and of a respectable spectral resolution) should allow us to fold into our analysis a self-consistent dynamical model for the central kinematics (e.g. based on Jeans equations; Magorrian 1999; Cappellari 2008), which will be also very sensitive to the age of the disc. For instance, at a given disc-light contribution, choosing an older stellar population for the disc will mean considering a more massive nuclear disc that will imprint a larger rotation velocity to the disc stars in the models, whereas picking a very young age will translate into a disc dynamics almost entirely determined by the gravitational potential of the bulge.

If our ability to constrain the stellar age of nearby NSDs seem set to improve in the near future, steps will also have to be made on a more theoretical side in order to better understand the implications of such age estimates. In particular, it will be paramount to assess the extent to which NSDs are fragile to merger episodes, so that the presence of an NSDs can be firmly translated into a maximum mass ratio for any accretion event that could have followed the formation of the disc. At the same time, it will also be interesting to follow the disruption of NSDs during more dramatic encounters, looking for instance for the possible kinematic signature of the past presence of such structures. Progress in this direction has already been made by Sarzi et al. (2015) using a relatively large set of numerical simulations, which show not only how NSDs emerge relatively unscathed from minor mergers (e.g. for a 1–10 mass ratio or less) but also that a central rotating structure could still be present at the end of more important interactions that leave no photometric trace of the NSD. Although encouraging, these results are still based on simple initial conditions mimicking the final phases of a merger event and which always lead the central black hole of the satellite galaxy to sink towards the centre, whereas this may not always be the case as we already noted. More comprehensive simulations are needed to fully understand both the origin of NSDs (Portaluri et al. 2013; Cole et al. 2014) and their fragility against minor mergers, possibly shedding also more light on the origin of kinematically decoupled central structures and the possible link to past central discs.

Finally, we note that the advantage of knowing a priori the stellar light contribution of a given stellar subpopulation to the optical spectra of a galaxy may be used to constrain also the stellar age of other kinds of galactic components beside NSDs, such as more extended discs (see, e.g. Johnston et al. 2012; Coccato, Iodice & Arnaboldi 2014; Johnston, Aragón-Salamanca & Merrifield 2014; Coccato et al. 2015), nuclear rings or other photometrically distinguishable structures.

ACKNOWLEDGEMENTS

Q12

REFERENCES

Anguita T., Faure C., Yonehara A., Wambsganss J., Kneib J.-P., Covone G., Alloin D., 2008, A&A, 481, 615
Bacon R. et al., 2010, Proc. SPIE, 7735, 7
Balcells M., Quinn P. J., 1990, ApJ, 361, 381
Bender R., Saglia R. P., Gerhard O. E., 1994, MNRAS, 269, 785

Binney J., 1978, MNRAS, 183, 501
Bois M. et al., 2011, MNRAS, 416, 1654
Böker T., Laine S., van der Marel R. P., Sarzi M., Rix H.-W., Ho L. C., Shields J. C., 2002, AJ, 123, 1389
Böker T., Sarzi M., McLaughlin D. E., van der Marel R. P., Rix H.-W., Ho L. C., Shields J. C., 2004, AJ, 127, 105
Bournaud F., 2011, EAS Publ. Ser., 51, 107
Callegari S., Mayer L., Kazantzidis S., Colpi M., Governato F., Quinn T., Wadsley J., 2009, ApJ, 696, L89
Callegari S., Kazantzidis S., Mayer L., Colpi M., Bellovary J. M., Quinn T., Wadsley J., 2011, ApJ, 729, 85
Calzetti D., Armus L., Bohlin R. C., Kinney A. L., Koornneef J., Storchi-Bergmann T., 2000, ApJ, 533, 682
Cappellari M., 2008, MNRAS, 390, 71
Cappellari M., Emsellem E., 2004, PASP, 116, 138
Cappellari M. et al., 2007, MNRAS, 379, 418
Cappellari M. et al., 2011, MNRAS, 413, 813
Cappellari M. et al., 2013, MNRAS, 432, 1709
Coccato L., Iodice E., Arnaboldi M., 2014, A&A, 569, A83
Coccato L. et al., 2015, MNRAS, submitted
Cole D. R., Debattista V. P., Erwin P., Earp S. W. F., Roškar R., 2014, MNRAS, 445, 3352
Corsini E. M., Méndez-Abreu J., Pastorello N., Dalla Bontà E., Morelli L., Beifiori A., Pizzella A., Bertola F., 2012, MNRAS, 423, L79
Corsini E. M., Morelli L., Pastorello N., Dalla Bontà E., Pizzella A., Portaluri E., 2016, MNRAS, preprint (arXiv:1511.08219)
Darg D. W. et al., 2010, MNRAS, 401, 1043
Davies R. L., Efstathiou G., Fall S. M., Illingworth G., Schechter P. L., 1983, ApJ, 266, 41
De Lucia G., Springel V., White S. D. M., Croton D., Kauffmann G., 2006, MNRAS, 366, 499
de Zeeuw P. T. et al., 2002, MNRAS, 329, 513
Di Matteo P., Combes F., Melchior A.-L., Semelin B., 2008, A&A, 477, 437
Emsellem E. et al., 2004, MNRAS, 352, 721
Emsellem E. et al., 2007, MNRAS, 379, 401
Emsellem E. et al., 2011, MNRAS, 414, 888
González J. J., 1993, PhD thesis, Univ. California, Santa Cruz
Hau G. K. T., Carter D., Balcells M., 1999, MNRAS, 306, 437
Hernquist L., Barnes J. E., 1991, Nature, 354, 210
Illingworth G., 1977, ApJ, 218, L43
Jesseit R., Cappellari M., Naab T., Emsellem E., Burkert A., 2009, MNRAS, 397, 1202
Johnston E. J., Aragón-Salamanca A., Merrifield M. R., Bedregal A. G., 2012, MNRAS, 422, 2590
Johnston E. J., Aragón-Salamanca A., Merrifield M. R., 2014, MNRAS, 441, 333
Khochfar S., Burkert A., 2006, A&A, 445, 403
Khochfar S., Silk J., 2006, MNRAS, 370, 902
Khochfar S. et al., 2011, MNRAS, 417, 845
Kuntschner H. et al., 2010, MNRAS, 408, 97
Le Fèvre O. et al., 2003, in Iye M., Moorwood A. F. M., eds, Proc. SPIE Conf. Ser. Vol. 4841, Instrument Design and Performance for Optical/Infrared Ground-based Telescopes. SPIE, Bellingham, p. 1670
Ledo H. R., Sarzi M., Dotti M., Khochfar S., Morelli L., 2010, MNRAS, 407, 969
Magorrian J., 1999, MNRAS, 302, 530
Maraston C., 2005, MNRAS, 362, 799
Maraston C., Strömbäck G., 2011, MNRAS, 418, 2785
Morelli L. et al., 2004, MNRAS, 354, 753
Morelli L., Cesetti M., Corsini E. M., Pizzella A., Dalla Bontà E., Sarzi M., Bertola F., 2010, A&A, 518, A32
Naab T. et al., 2014, MNRAS, 444, 3357
Pizzella A., Corsini E. M., Morelli L., Sarzi M., Scarlata C., Stiavelli M., Bertola F., 2002, ApJ, 573, 131
Portaluri E., Corsini E. M., Morelli L., Hartmann M., Dalla Bontà E., Debattista V. P., Pizzella A., 2013, MNRAS, 433, 434
Rossa J., van der Marel R. P., Böker T., Gerssen J., Ho L. C., Rix H.-W., Shields J. C., Walcher C.-J., 2006, AJ, 132, 1074
Sánchez-Blázquez P. et al., 2006, MNRAS, 371, 703
Sarzi M., Rix H.-W., Shields J. C., Ho L. C., Barth A. J., Rudnick G., Filippenko A. V., Sargent W. L. W., 2005, ApJ, 628, 169
Sarzi M. et al., 2006, MNRAS, 366, 1151
Sarzi M. et al., 2010, MNRAS, 402, 2187
Sarzi M., Ledo H. R., Dotti M., 2015, MNRAS, in press
Scorza C., Bender R., 1995, A&A, 293, 20
Thomas D., Maraston C., Bender R., Mendes de Oliveira C., 2005, ApJ, 621, 673
Thomas D., Maraston C., Schawinski K., Sarzi M., Silk J., 2010, MNRAS, 404, 1775
Toomre A., 1977, in Tinsley B. M., Larson R. B., eds, Evolution of Galaxies and Stellar Populations. Yale University Observatory, New Haven, p. 401
van den Bosch F. C., Ferrarese L., Jaffe W., Ford H. C., O'Connell R. W., 1994, AJ, 108, 1579
Vazdekis A., Sánchez-Blázquez P., Falcón-Barroso J., Cenarro A. J., Beasley M. A., Cardiel N., Gorgas J., Peletier R. F., 2010, MNRAS, 404, 1639
Walcher C. J. et al., 2005, ApJ, 618, 237
Weijmans A.-M. et al., 2014, MNRAS, 444, 3340

This paper has been typeset from a TEX/LATEX file prepared by the author.

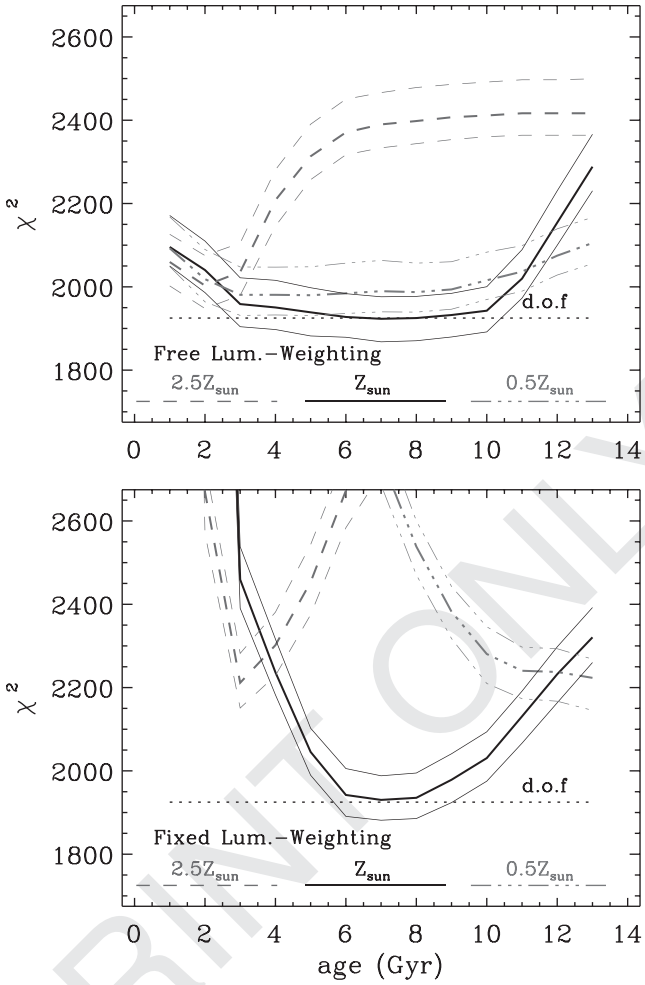

Figure 1. Simulations showing the accuracy in recovering the age of a 7-Gyr-old disc population that is embedded in a 13-Gyr-old bulge population. The bulge and disc populations contribute with the same broad-band flux between 4500 and 5500 Å to the input model, and are represented by single-age stellar population models of solar metallicity from Maraston & Strömbäck (2011), covering the entire wavelength range of our VIMOS observations (Section 3). Different amounts of kinematical broadening were also included in the bulge and disc models (σ = 200 and 100 km s^{-1}), and statistical fluctuations were added to simulate an S/N $\sim$ 100. In both panels, the thick solid line shows the average quality of the fit to the input model as disc single-age models of increasing ages are combined with the right, 13-Gyr-old, bulge population model, which mimics the situation where the bulge stellar properties have been previously constrained from off-centred observations. The thin solid lines indicate the 1σ fluctuation that is derived by fitting different realizations of the input model. The dashed and dot–dashed lines show the quality of the fits obtained while considering disc populations of supersolar and subsolar metallicities. On the left-hand panel, the relative contribution to the fit of the bulge and disc populations is left free to vary, whereas on the right-hand panel each component is constrained to contribute the same broad-band flux in the 4500–5500 Å range as in the input model. In both cases, the kinematic broadening of the templates is also freely adjusted during the fit. The comparison between χ^2 curves in the left- and right-hand panels illustrates how knowing in advance the disc-light contribution allows one to recover the correct disc age and metallicity, whereas without such an initial clue estimating the disc age and metallicity would be complicated by the well-known degeneracy between these two parameters.

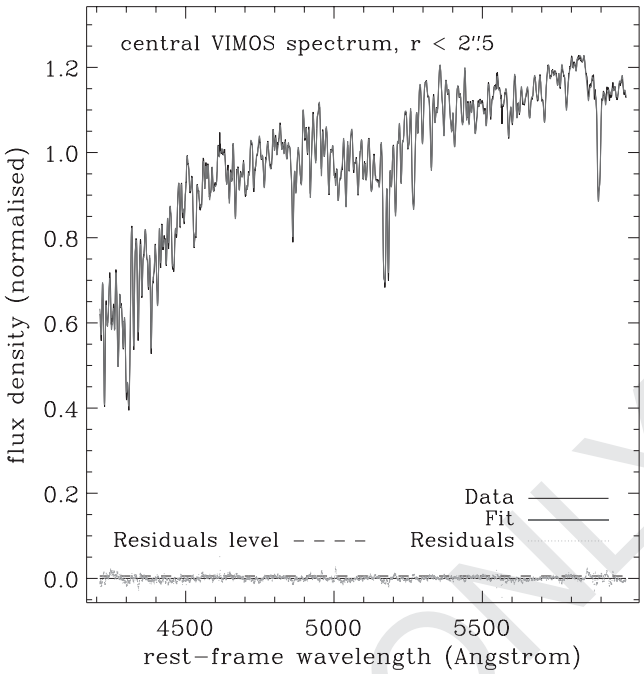

Figure 3. Central 5 arcsec VIMOS spectrum of NGC 4458 and our best pPXF fit using the entire MILES spectral library. The level of fluctuations in the residuals of this fit correspond to an average value of 175 for the signal over residual-noise ratio.

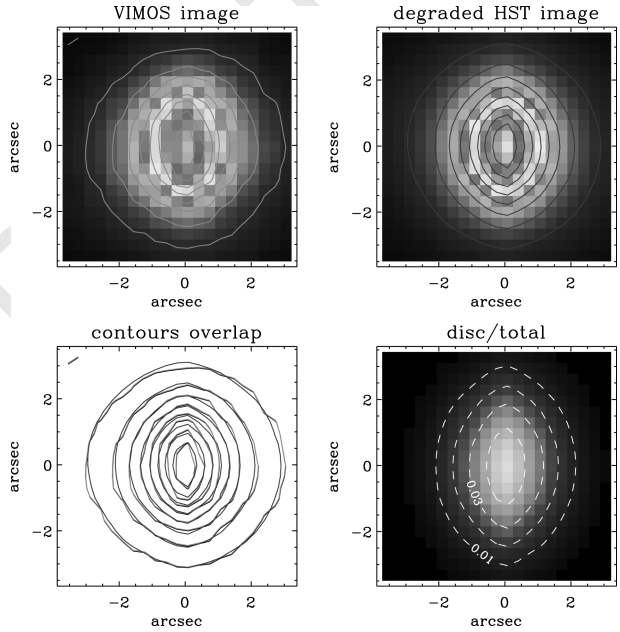

Figure 4. Upper panels: central parts of the VIMOS reconstructed image of NGC 4458 (left) and the same for the *F*555*W* Wide Field Planetary Camera 2 image, once degraded to match the spatial resolution of VIMOS and resampled within the 0.33 arcsec× 0.33 arcsec resolution elements of the high-resolution configuration of VIMOS (right). Lower left: overlap of the surface brightness contours for the VIMOS and degraded *HST* image (in light and dark grey lines, respectively), which are also shown in the corresponding upper panels. Lower right: map for the disc-to-total light ratio computed from the *HST* degraded image shown in the upper-right panel and a similarly convolved and resampled version for the image of the best-fitting disc model that was obtained during the Scorza & Bender disc–bulge decomposition of Morelli et al. (2004). The dashed contours on this last image show the level of disc-light contribution in the VIMOS spaxels (but see the text). Note that the major axis of NGC 4458 and its nuclear disc runs nearly parallel to the *x*-axis of the VIMOS cube, and the vertical elongation shown here is the results of the rather elongated point-spread function of VIMOS and the steep profile of the intrinsic surface brightness of this galaxy.

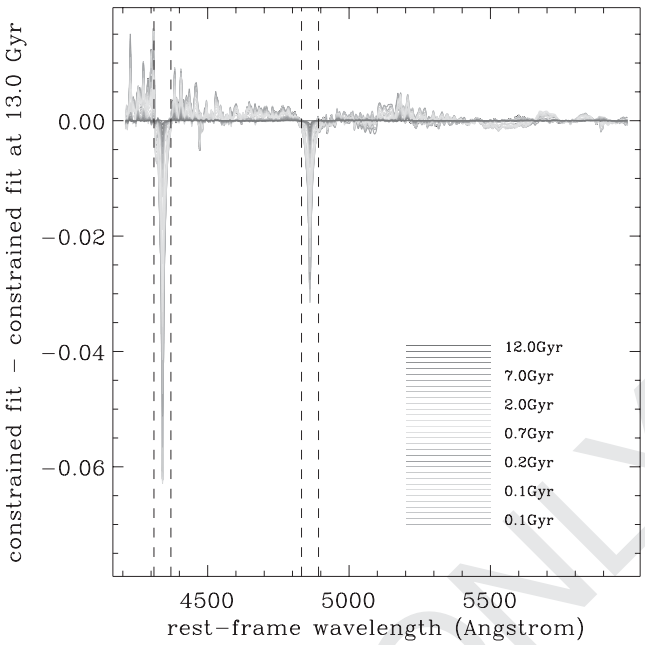

Figure 6. Difference between the best-fitting constrained fit model, which features a 12.6-Gyr-old disc, and all other constrained fits including different single-age disc templates. The largest deviations are observed within the spectral regions identified by the vertical dashed lines, which correspond to the age-sensitive H δ and H β stellar absorption features (at 4340 and 4861 Å, respectively). Nearly 90 per cent of the quadratic difference (relevant for comparing model χ^2 values) with the youngest disc model is contained across these 30 Å-wide spectral windows, with this fraction lowering to ∼40 per cent when comparing our best model with other models featuring old discs.

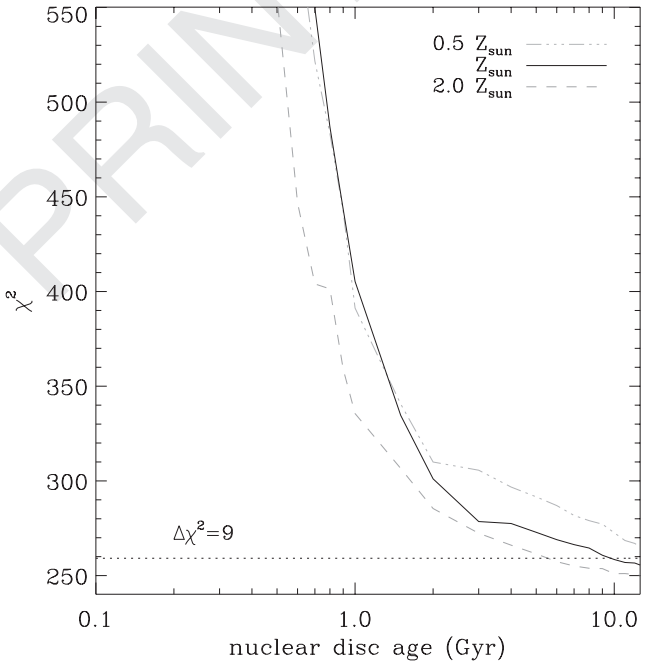

Figure 7. Final stellar age estimate for the NSD of NGC 4458. Similar to Fig. 5, but now based only on constrained fit model featuring single-age disc templates of different metallicities (solid lines for solar values, dot–dashed and dashed for half and twice solar values, respectively) and while assessing the quality of the fits within the H δ and H β spectral windows shown in Fig. 6. All plotted χ^2 values within this spectral region have been computed after rescaling all flux-density errors assuming that the best constrained fit model would yield a χ^2=NDOF across the *entire* spectrum. A $\Delta\chi^2 = 9$ threshold set from the best χ^2 value obtained within the H δ and H β windows indicate that at best, when considering populations of super-Solar metallicity, the nuclear disc could have formed as recently as ∼5–6 Gyr ago.

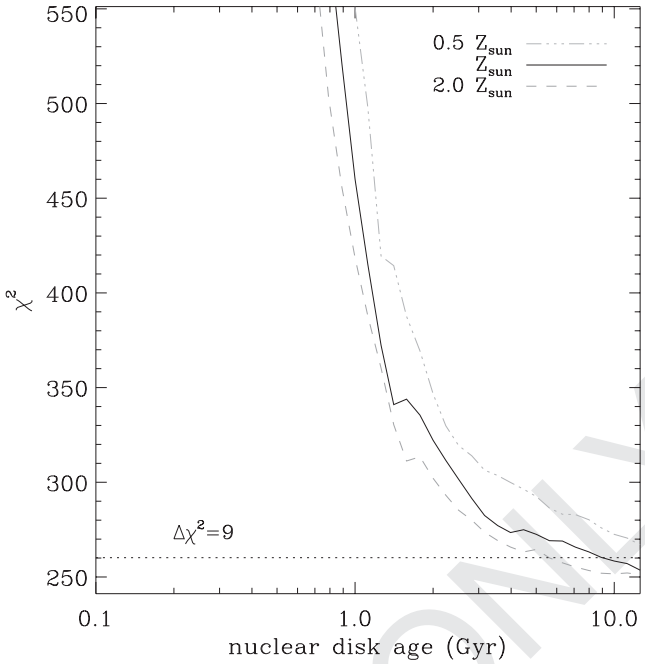

Figure 8. Similar to Fig. 7 but now while adopting the single-age models of Vazdekis et al. (2010), based also on the MILES stellar library.

List of astronomical key words (updated 2013 July)

This list is common to *Monthly Notices of the Royal Astronomical Society, Astronomy and Astrophysics*, and *The Astrophysical Journal*. In order to ease the search, the key words are subdivided into broad categories. No more than *six* subcategories altogether should be listed for a paper.

The subcategories in boldface containing the word 'individual' are intended for use with specific astronomical objects; these should never be used alone, but always in combination with the most common names for the astronomical objects in question. Note that each object counts as one subcategory within the allowed limit of six.

The parts of the key words in italics are for reference only and should be omitted when the key words are entered on the manuscript.

General

editorials, notices
errata, addenda
extraterrestrial intelligence
history and philosophy of astronomy
miscellaneous
obituaries, biographies
publications, bibliography
sociology of astronomy
standards

Physical data and processes

acceleration of particles
accretion, accretion discs
asteroseismology
astrobiology
astrochemistry
astroparticle physics
atomic data
atomic processes
black hole physics
chaos
conduction
convection
dense matter
diffusion
dynamo
elementary particles
equation of state
gravitation
gravitational lensing: strong
gravitational lensing: weak
gravitational lensing: micro
gravitational waves
hydrodynamics
instabilities
line: formation
line: identification
line: profiles
magnetic fields
magnetic reconnection
(magnetohydrodynamics) MHD
masers
molecular data
molecular processes
neutrinos
nuclear reactions, nucleosynthesis, abundances
opacity
plasmas
polarization
radiation: dynamics
radiation mechanisms:general
radiation mechanisms: non-thermal
radiation mechanisms: thermal
radiative transfer
relativistic processes
scattering
shock waves
solid state: refractory
solid state: volatile
turbulence
waves

Astronomical instrumentation, methods and techniques

atmospheric effects
balloons
instrumentation: adaptive optics
instrumentation: detectors
instrumentation: high angular resolution
instrumentation: interferometers
instrumentation: miscellaneous
instrumentation: photometers
instrumentation: polarimeters
instrumentation: spectrographs
light pollution
methods: analytical
methods: data analysis
methods: laboratory: atomic
methods: laboratory: molecular
methods: laboratory: solid state
methods: miscellaneous
methods: numerical
methods: observational
methods: statistical
site testing
space vehicles
space vehicles: instruments
techniques: high angular resolution
techniques: image processing
techniques: imaging spectroscopy
techniques: interferometric
techniques: miscellaneous
techniques: photometric
techniques: polarimetric
techniques: radar astronomy
techniques: radial velocities

techniques: spectroscopic
telescopes

Astronomical data bases

astronomical data bases: miscellaneous
atlases
catalogues
surveys
virtual observatory tools

Astrometry and celestial mechanics

astrometry
celestial mechanics
eclipses
ephemerides
occultations
parallaxes
proper motions
reference systems
time

The Sun

Sun: abundances
Sun: activity
Sun: atmosphere
Sun: chromosphere
Sun: corona
Sun: coronal mass ejections (CMEs)
Sun: evolution
Sun: faculae, plages
Sun: filaments, prominences
Sun: flares
Sun: fundamental parameters
Sun: general
Sun: granulation
Sun: helioseismology
Sun: heliosphere
Sun: infrared
Sun: interior
Sun: magnetic fields
Sun: oscillations
Sun: particle emission
Sun: photosphere
Sun: radio radiation
Sun: rotation
(Sun:) solar–terrestrial relations
(Sun:) solar wind
(Sun:) sunspots
Sun: transition region
Sun: UV radiation
Sun: X-rays, gamma-rays

Planetary systems

comets: general
comets: individual: . . .
Earth
interplanetary medium
Kuiper belt: general
Kuiper belt objects: individual: . . .
meteorites, meteors, meteoroids
minor planets, asteroids: general
minor planets, asteroids: individual: . . .
Moon
Oort Cloud
planets and satellites: atmospheres
planets and satellites: aurorae
planets and satellites: composition
planets and satellites: detection
planets and satellites: dynamical evolution and stability
planets and satellites: formation
planets and satellites: fundamental parameters
planets and satellites: gaseous planets
planets and satellites: general
planets and satellites: individual: . . .
planets and satellites: interiors
planets and satellites: magnetic fields
planets and satellites: oceans
planets and satellites: physical evolution
planets and satellites: rings
planets and satellites: surfaces
planets and satellites: tectonics
planets and satellites: terrestrial planets
planet–disc interactions`
planet–star interactions
protoplanetary discs
zodiacal dust

Stars
stars: abundances
stars: activity
stars: AGB and post-AGB
stars: atmospheres
(stars:) binaries *(including multiple)*: close
(stars:) binaries: eclipsing
(stars:) binaries: general
(stars:) binaries: spectroscopic
(stars:) binaries: symbiotic
(stars:) binaries: visual
stars: black holes
(stars:) blue stragglers
(stars:) brown dwarfs
stars: carbon
stars: chemically peculiar
stars: chromospheres
(stars:) circumstellar matter
stars: coronae
stars: distances
stars: dwarf novae
stars: early-type
stars: emission-line, Be
stars: evolution
stars: flare
stars: formation
stars: fundamental parameters
(stars:) gamma-ray burst: general
(stars:) **gamma-ray burst: individual: . . .**
stars: general
(stars:) Hertzsprung–Russell and colour–magnitude diagrams
stars: horizontal branch
stars: imaging
stars: individual: . . .

stars: interiors
stars: jets
stars: kinematics and dynamics
stars: late-type
stars: low-mass
stars: luminosity function, mass function
stars: magnetars
stars: magnetic field
stars: massive
stars: mass-loss
stars: neutron
(stars:) novae, cataclysmic variables
stars: oscillations *(including pulsations)*
stars: peculiar *(except chemically peculiar)*
(stars:) planetary systems
stars: Population II
stars: Population III
stars: pre-main-sequence
stars: protostars
(stars:) pulsars: general
(stars:) **pulsars: individual: . . .**
stars: rotation
stars: solar-type
(stars:) starspots
stars: statistics
(stars:) subdwarfs
(stars:) supergiants
(stars:) supernovae: general
(stars:) **supernovae: individual: . . .**
stars: variables: Cepheids
stars: variables: δ Scuti
stars: variables: general
stars: variables: RR Lyrae
stars: variables: S Doradus
stars: variables: T Tauri, Herbig Ae/Be
(stars:) white dwarfs
stars: winds, outflows
stars: Wolf–Rayet

Interstellar medium (ISM), nebulae

ISM: abundances
ISM: atoms
ISM: bubbles
ISM: clouds
(ISM:) cosmic rays
(ISM:) dust, extinction
ISM: evolution
ISM: general
(ISM:) H II regions
(ISM:) Herbig–Haro objects
ISM: individual objects: . . .
(except planetary nebulae)
ISM: jets and outflows
ISM: kinematics and dynamics
ISM: lines and bands
ISM: magnetic fields
ISM: molecules
(ISM:) planetary nebulae: general
(ISM:) **planetary nebulae: individual: . . .**
(ISM:) photodissociation region (PDR)
ISM: structure
ISM: supernova remnants

The Galaxy

Galaxy: abundances
Galaxy: bulge
Galaxy: centre
Galaxy: disc
Galaxy: evolution
Galaxy: formation
Galaxy: fundamental parameters
Galaxy: general
(Galaxy:) globular clusters: general
(Galaxy:) **globular clusters: individual: . . .**
Galaxy: halo
Galaxy: kinematics and dynamics
(Galaxy:) local interstellar matter
Galaxy: nucleus
(Galaxy:) open clusters and associations: general
(Galaxy:) **open clusters and associations: individual: . . .**
(Galaxy:) solar neighbourhood
Galaxy: stellar content
Galaxy: structure

Galaxies

galaxies: abundances
galaxies: active
(galaxies:) BL Lacertae objects: general
(galaxies:) **BL Lacertae objects: individual: . . .**
galaxies: bulges
galaxies: clusters: general
galaxies: clusters: individual: . . .
galaxies: clusters: intracluster medium
galaxies: distances and redshifts
galaxies: dwarf
galaxies: elliptical and lenticular, cD
galaxies: evolution
galaxies: formation
galaxies: fundamental parameters
galaxies: general
galaxies: groups: general
galaxies: groups: individual: . . .
galaxies: haloes
galaxies: high-redshift
galaxies: individual: . . .
galaxies: interactions
(galaxies:) intergalactic medium
galaxies: irregular
galaxies: ISM
galaxies: jets
galaxies: kinematics and dynamics
(galaxies:) Local Group
galaxies: luminosity function, mass function
(galaxies:) Magellanic Clouds
galaxies: magnetic fields
galaxies: nuclei
galaxies: peculiar
galaxies: photometry
(galaxies:) quasars: absorption lines
(galaxies:) quasars: emission lines
(galaxies:) quasars: general
(galaxies:) **quasars: individual: . . .**
(galaxies:) quasars: supermassive black holes
galaxies: Seyfert

galaxies: spiral
galaxies: starburst
galaxies: star clusters: general
galaxies: star clusters: individual: . . .
galaxies: star formation
galaxies: statistics
galaxies: stellar content
galaxies: structure

Cosmology

(cosmology:) cosmic background radiation
(cosmology:) cosmological parameters
cosmology: miscellaneous
cosmology: observations
cosmology: theory
(cosmology:) dark ages, reionization, first stars
(cosmology:) dark energy
(cosmology:) dark matter
(cosmology:) diffuse radiation
(cosmology:) distance scale
(cosmology:) early Universe
(cosmology:) inflation
(cosmology:) large-scale structure of Universe
(cosmology:) primordial nucleosynthesis

Resolved and unresolved sources as a function of wavelength

gamma-rays: diffuse background
gamma-rays: galaxies
gamma-rays: galaxies: clusters
gamma-rays: general
gamma-rays: ISM
gamma-rays: stars
infrared: diffuse background
infrared: galaxies
infrared: general
infrared: ISM
infrared: planetary systems
infrared: stars
radio continuum: galaxies
radio continuum: general
radio continuum: ISM
radio continuum: planetary systems
radio continuum: stars
radio lines: galaxies
radio lines: general
radio lines: ISM
radio lines: planetary systems
radio lines: stars
submillimetre: diffuse background
submillimetre: galaxies
submillimetre: general
submillimetre: ISM
submillimetre: planetary systems
submillimetre: stars
ultraviolet: galaxies
ultraviolet: general
ultraviolet: ISM
ultraviolet: planetary systems
ultraviolet: stars
X-rays: binaries
X-rays: bursts
X-rays: diffuse background
X-rays: galaxies
X-rays: galaxies: clusters
X-rays: general
X-rays: individual: . . .
X-rays: ISM
X-rays: stars